

A unified finite volume framework for phase-field simulations of an arbitrary number of fluid phases

Milad Bagheri¹  | Bastian Stumpf²  | Ilia V. Roisman²  |
Abdolrahman Dadvand³  | Martin Wörner⁴  | Holger Marschall¹ 

¹Department of Mathematics,
Computational Multiphase Flow,
Technische Universität Darmstadt,
Darmstadt, Germany

²Institute of Fluid Mechanics and
Aerodynamics, Technische Universität
Darmstadt, Darmstadt, Germany

³Faculty of Mechanical Engineering,
Urmia University of Technology,
Urmia, Iran

⁴Institute of Catalysis Research and
Technology, Karlsruhe Institute of
Technology (KIT), Karlsruhe, Germany

Correspondence

Milad Bagheri and Holger Marschall,
Department of Mathematics,
Computational Multiphase Flow,
Technische Universität Darmstadt,
Darmstadt, 64287, Germany.

Email: milad.bagheri@tu-darmstadt.de
and holger.marschall@tu-darmstadt.de

Funding information

Deutsche Forschungsgemeinschaft, Grant/
Award Number: 237267381 - TRR 150

Abstract

While the phase-field methodology is widely adopted for simulating two-phase flows, the simulation of an arbitrary number ($N \geq 2$) of fluid phases at physical fidelity is non-trivial and requires special attention concerning mathematical modelling, numerical discretization, and solution algorithm. We present our most recent work with a focus on validation for multiple immiscible, incompressible, and isothermal phases, enhancing further our library for diffuse interface phase-field interface capturing methods in OpenFOAM (FOAM-extend 4.0/4.1). The phase-field method is an energetic variational formulation based on the work of Cahn and Hilliard where the interface is composed of a physical diffuse layer resembling realistic interfaces. The evolution of the phases is then governed by the minimization of the free energy of the system. The accuracy of the method is demonstrated for a number of test problems, including a floating liquid lens, bubble rise in two stratified layers, and drop impact onto thin liquid film.

KEYWORDS

Cahn–Hilliard Navier–Stokes, multiphase flows, phase-field

1 | INTRODUCTION

Numerical simulation of technically relevant applications of fluid dynamics often extends beyond a two-phase problem formulation. In numerous processes, more than two phases co-exist with multiple fluid interfaces dynamically evolving. Of particular interest to this study are applications linked to drop-film-interactions in internal combustion engines. In such combustion processes, fuel droplets collide with a thin layer of lubricating oil film on the piston that might

weaken/change the oil's lubricating properties and cause combustion of a fuel–oil mixture instead of a pure fuel combustion. A fundamental understanding of such a complex and dynamic process requires detailed numerical simulation of the physics involved during the impact process that includes more than two phases. To this end, we have extended our two-phase diffuse interface modelling library for phase-field interface capturing simulations to cover more than two immiscible, incompressible, and isothermal phases. Here, we refer to a region of matter surrounded by an adjacent

This is an open access article under the terms of the [Creative Commons Attribution](https://creativecommons.org/licenses/by/4.0/) License, which permits use, distribution and reproduction in any medium, provided the original work is properly cited.

© 2022 The Authors. The *Canadian Journal of Chemical Engineering* published by Wiley Periodicals LLC on behalf of Canadian Society for Chemical Engineering.

medium as a phase, which in the present work can be liquid or gaseous fluid regions, respectively.

The building block of our approach is the phase-field interface capturing method, based on a diffuse-interface model, where the system is described using one field variable in the case of a two-phase flow or multiple field variables in the case of a multiphase flow problem. Unlike interface capturing methods based on sharp-interface modelling, such as volume-of-fluid (VOF) or level-set (LS), the composition profile across the interface in the phase-field method is sigmoid in shape, based on the work of Cahn and Hilliard,^[1] that reflects a physically diffuse profile. The ingenuity of this method stems from the fact that the free energy of a non-homogeneous system contains interfacial energy-related effects in the form of composition gradient, and the system evolves by minimization of its free energy. This is different from the aforementioned methods, which underlie a continuum mechanical rationale; see the work of Brackbill et al.,^[2] for instance. The advantages and challenges of the phase-field methodology are set out and discussed extensively in the work of Feng et al.^[3]

The fluid dynamics of a system of multiple fluid phases is governed by the coupled Cahn–Hilliard Navier–Stokes equations. For the mathematical foundation for immiscible, incompressible, and isothermal two-phase flows, one can refer to many available treatises in the literature, such as the works of Lowengrub and Truskinovsky,^[4] Jacqmin,^[5] Jacqmin,^[6] Liu and Shen,^[7] Yue et al.,^[8] and Ding et al.^[9] Extension from two-phase to ternary-phase systems were proposed for instance in the works of Kim and Lowengrub,^[10] Boyer and Lapuerta,^[11] Kim,^[12] Boyer et al.,^[13] and He et al.^[14] Such models for ternary systems are available in proprietary software, like, for instance, in the microfluidics module of COMSOL Multiphysics software that is described in the COMSOL Multiphysics User’s guide^[15] based on the work of Boyer et al.^[13] Open-source code for the simulation of ternary systems has been made available under the numerical simulation platform PELICANS.^[16] The model in Boyer et al.^[13] was subjected to a study pursued in the work of Řehoř et al.^[17] and implemented using the FEniCS Project.^[18]

Extending the model formulation to systems containing an arbitrary number of fluid phases (i.e., the general case of $N > 2$ phases) is non-trivial and indeed subject to ongoing research building on continuous efforts during the last decade.^[19–29] One central challenge for an N -phase model to be of physical fidelity resides in the requirement to honour thermodynamic and reduction consistency likewise. Based on the pioneering work of Boyer and Minjeaud,^[20] Dong^[24] presented for the first time a fully reduction-consistent model formulation, that

is, an N -phase model, which reduces to the established two-phase model, when only two phases are initialized to co-exist in multiphase setups. Their N -phase model was moreover reported to be thermodynamically consistent, that is, to obey conservation of mass, conservation of momentum, the second law of thermodynamics, and Galilean invariance.^[24] Nevertheless, the model of Huang et al.^[27] then contains several modifications to fulfil consistency conditions and further improve the work of Dong.^[24] Differences are indeed subtle, and these papers have paved the avenue towards the practical deployment of the phase-field method for multiphase flow simulations. On these bases, we have implemented a versatile diffuse-interface model library for multiple phases using the finite volume method (FVM) with support for unstructured meshes of general topology in OpenFOAM (FOAM-extend 4.0/4.1). In future work, we will aim at the deployment for simulating multiphase flows in geometrically complex domains such as porous media or fibre mats. This work shall demonstrate our validation efforts for a broad bandwidth of different literature-known numerical tests and benchmarks for multiphase flows including a floating liquid lens, bubble rise in two stratified layers, and drop impact onto thin liquid film.

2 | MATHEMATICAL FORMULATION

2.1 | Two-phase Cahn–Hilliard Navier–Stokes equations

The flow of two immiscible, incompressible, and isothermal Newtonian fluid phases is governed by the coupled Cahn–Hilliard Navier–Stokes equations. Here, only a single phase-field variable $c \in [-1, 1]$ (volume fraction contrast) has to be used to discriminate the presence of the phases. The concentration in the bulk phases is represented by $c = \pm 1$ and the position of the fluid interface can be represented as the zero iso-surface $c = 0$. Following the work of Cahn and Hilliard,^[1] the total free energy (Helmholtz free energy functional) of this system consists of the sum of the bulk and the gradient energy contributions, which can be written as^[8]:

$$F(c, \nabla c) = \int_{\Omega} \lambda \left\{ \frac{\Psi(c)}{\varepsilon^2} + \frac{|\nabla c|^2}{2} \right\} d\Omega, \quad (1)$$

where Ω is the fluid domain, λ is the interfacial mixing energy density parameter, ε is the capillary width, and $\Psi(c)$ is the so-called double-well potential which can be phenomenologically modelled according to Ginzburg and

Landau,^[30] that is, $\Psi(c) = \frac{1}{4}(c^2 - 1)^2$. Assuming a planar interface and equilibrium conditions, the interfacial mixing energy density parameter λ can be shown to be $\lambda = \frac{3}{2\sqrt{2}}\sigma\epsilon$ where σ is the interfacial tension coefficient.

The evolution/kinetics of the system is described by the minimization of free energy through a variational procedure,^[1] which leads to the chemical potential Φ of the system:

$$\Phi = \frac{\delta F}{\delta c} = \lambda \left[\frac{\Psi'(c)}{\epsilon^2} - \nabla^2 c \right], \quad (2)$$

where $\Psi'(c)$ is the first derivative of the double-well potential with respect to the order parameter c . Using the Ginzburg and Landau double-well potential, $\Psi'(c) = c^3 - c$. From this, the equilibrium interface profile can be obtained when requiring $\Phi = 0$, which yields:

$$c(x) = \tanh\left(\frac{x}{\sqrt{2}\epsilon}\right), \quad (3)$$

where x is the local coordinate normal to the interface.

The fluid dynamics of two immiscible incompressible phases are then governed by the Cahn–Hilliard equation being coupled with the Navier–Stokes equation following the work of Jacqmin,^[5] viz.:

$$\partial_t c + \nabla \cdot (c\mathbf{u}) = -\nabla \cdot \mathbf{J}, \quad (4a)$$

$$\nabla \cdot \mathbf{u} = 0, \quad (4b)$$

$$\begin{aligned} \partial_t(\rho_c \mathbf{u}) + \nabla \cdot (\rho_c \mathbf{u} \otimes \mathbf{u}) &= -\nabla \tilde{p} \\ + \nabla \cdot \boldsymbol{\tau} + \rho_c \mathbf{g} - \nabla \cdot (\mathbf{u} \otimes \mathbf{J}) &+ \mathbf{f}_s, \end{aligned} \quad (4c)$$

where t is the time, \mathbf{u} is the divergence-free velocity field, and ρ_c and μ_c are the volumetric average density and dynamic viscosity of the two fluids, given as $\rho_c = \frac{1+c}{2}\rho_1 + \frac{1-c}{2}\rho_2$ and $\mu_c = \frac{1+c}{2}\mu_1 + \frac{1-c}{2}\mu_2$. The term \tilde{p} denotes a modified pressure, since parts of the known Korteweg tensor term accounting for interfacial capillarity have been absorbed into the pressure gradient term. For Newtonian fluids, the viscous stress tensor is $\boldsymbol{\tau} = \mu_c(\nabla \mathbf{u} + (\nabla \mathbf{u})^T)$. The gravitational acceleration is \mathbf{g} and \mathbf{J} is the phase-field flux that generalizes the Fick's law as $\mathbf{J} = -M \nabla \Phi$, with M being the mobility parameter. The term $\mathbf{f}_s = \Phi \nabla c$ models the capillarity of the diffusive interfaces on the basis of the Korteweg stress tensor.^[31] Note that (Equation (4a)) is a fourth-order non-linear parabolic partial differential equation with respect to c , which renders it challenging to solve numerically.^[32]

2.2 | N-phase Cahn–Hilliard Navier–Stokes equations

The evolution of the order parameters c_p , $1 \leq p \leq N$, for N immiscible fluids is governed by the Cahn–Hilliard transport equations, as^[20,33]:

$$\partial_t c_p + \nabla \cdot (c_p \mathbf{u}) = -\nabla \cdot \mathbf{J}_p. \quad (5)$$

Due to isochoric conditions (phase volume conservation), it applies for multiple phases that $\sum_{p=1}^N c_p = 2 - N$.

The phase-field flux in Equation (5) is:

$$\mathbf{J}_p = \sum_{q=1}^N -M_{p,q} \mathbf{Q}_{p,q}^m \nabla \Phi_q, \quad m=4, \quad (6)$$

where

$$\Phi_p = \sum_{q=1}^N \lambda_{p,q} \left[\frac{1}{\epsilon^2} (\Psi'_1(c_p) - \Psi'_2(c_p + c_q)) + \nabla^2 c_q \right], \quad 1 \leq p \leq N \quad (7)$$

is the chemical potential of phase p , and

$$M_{p,q} = \begin{cases} -M_0(1+c_p)(1+c_q), & p \neq q \\ M_0(1+c_p)(1-c_q), & p = q \end{cases}, \quad 1 \leq p, q \leq N \quad (8)$$

is the scalar mobility between phases p and q , where M_0 is a non-negative mobility constant. In recognition of the intuitive statement that the mobility should be tensorial,^[34] we devise $\mathbf{Q}_{p,q}$ in Equation (6) as a modified projection operator $\mathbf{I} - \mathbf{n}_p \otimes \mathbf{n}_p$, viz.^[34]:

$$\mathbf{Q}_{p,q} = \mathbf{I} - \frac{\epsilon^2 (\nabla c_p)^2}{\Psi_1(c_p) + \Psi_1(c_q) - \Psi_2(c_p + c_q)} (\mathbf{n}_p \otimes \mathbf{n}_p). \quad (9)$$

Note that in the sharp-interface-limit ($\epsilon \rightarrow 0$) the operator $\nabla \cdot M_{p,q} \nabla$ in Equation (5) reduces to the Laplace–Beltrami operator Δ_s in the asymptotic limit. Details about the exponent in Equation (6), which we choose to $m = 4$, are given in the work of Gugenberger et al.^[34] Using the potential according to Ginzburg and Landau,^[30] the phenomenological potential functions are $\Psi_1(c) = \frac{1}{4}(c^2 - 1)^2$ and $\Psi_2(c) = \frac{1}{4}c^2(c + 2)^2$.

The interfacial mixing energy density parameters $\lambda_{p,q}$ in Equation (7) are $\lambda_{p,q} = \frac{3}{2\sqrt{2}}\sigma_{p,q}\epsilon$, as a function of pairwise interfacial tension coefficients and capillary widths.

Here, the matrix $\{\lambda_{p,q}\}_{p,q=1}^N$ is symmetric and zero-diagonal. It should be noted that zero gradient (homogeneous Neumann) boundary conditions are used for both the order parameters and the chemical potentials on the computational boundaries in our work.

The coupling with the Navier–Stokes equations,

$$\begin{aligned} \nabla \cdot \mathbf{u} &= 0 \\ \partial_t(\rho_c \mathbf{u}) + \nabla \cdot (\rho_c \mathbf{u} \otimes \mathbf{u}) &= -\nabla \tilde{p} + \nabla \cdot \boldsymbol{\tau} \\ + \rho_c \mathbf{g} - \nabla \cdot (\mathbf{u} \otimes \mathbf{J}) + \mathbf{f}_s, \end{aligned} \quad (10)$$

is accomplished via constitutive models, which hold the order parameter and/or the chemical potential. The average density and dynamic viscosity are $\rho_c = \sum_{p=1}^N \rho_p \frac{c_p+1}{2}$ and $\mu_c = \sum_{p=1}^N \mu_p \frac{c_p+1}{2}$, respectively. The diffusive mass flux is $\mathbf{J} = (1/2) \sum_{p=1}^N \rho_p \mathbf{J}_p$. The pressure \tilde{p} is a modified pressure term,

$$\tilde{p} := p - \frac{e_F}{2}, \quad (11)$$

where

$$e_F := \sum_{p,q=1}^N \frac{\lambda_{p,q}}{2} \left(\frac{1}{\varepsilon^2} (\Psi_1(c_p) + \Psi_1(c_q) - \Psi_2(c_p + c_q)) - \nabla c_p \cdot \nabla c_q \right), \quad (12)$$

which is the total free energy density for N immiscible, incompressible, and isothermal phases. The chemical potentials Φ_p are determined through the variational derivative of the total free energy with respect to the order parameter. This results in the well-known Korteweg stress term, but in the formulation for a multiphase system. This term is transformed and partially absorbed into the pressure gradient term: $\frac{1}{2} \sum_{p,q=1}^N \nabla \cdot (\lambda_{p,q} \nabla c_p \otimes \nabla c_q) = \mathbf{f}_s - \nabla \frac{e_F}{2}$,

where $\mathbf{f}_s = \frac{1}{2} \sum_{p=1}^N \Phi_p \nabla c_p$.

3 | SOFTWARE DESCRIPTION, ALGORITHM, AND NUMERICAL SCHEMES

The diffuse-interface phase-field method for an arbitrary number of fluid phases, as described in Section 2.2 is

implemented in OpenFOAM (FOAM-extend 4.1) as model library used by a top-level solver referred to as `phaseFieldFoam`. OpenFOAM is a comprehensive open-source C++ library for computational continuum physics including computational fluid dynamics (CFD).^[35–37] The code structure follows a rigorous object-oriented and physics-guided development paradigm, which results in a versatile code design that is extendable towards coupled (multi-)physics applications.

The deprecated two-phase version of `phaseFieldFoam` has been extensively validated for different physics in the works of Cai et al.,^[38] Cai et al.,^[39] Fink et al.,^[40] Wörner et al.,^[41] Samkhaniani et al.,^[42] and Bagheri et al.^[43] and its solution algorithm is described in the work of Jamshidi et al.^[44] The algorithms for pressure–velocity coupling lean on other interface capturing approaches implemented in OpenFOAM and described in great detail in the work of Deshpande et al.^[45] and have been massively extended in our work to cope with high-fidelity solution of the coupled Cahn–Hilliard–Navier–Stokes equations for N immiscible, incompressible, and isothermal phases. The viscous stress tensor $\boldsymbol{\tau}$ implementation is generic in the sense that it allows the use of any fluid rheology model available in OpenFOAM. The interfacial Korteweg tensor term \mathbf{f}_s is implemented as a volumetric density, whereupon in the context of phase-field method it substantially reduces the parasitic/spurious currents by orders of magnitude when compared to methods based on sharp-interface models.^[5,44,46]

The basic structure of our diffuse-interface model library is depicted in Figure 1. It consists of two main base classes, namely, `multiphaseSystem` that includes constitutive models and `phaseFieldEquations` that includes the transport equations for the order parameters.

The pressure–velocity coupling is carried out using the PIMPLE algorithm, which is a combination of the Pressure Implicit with Splitting of Operator (PISO)^[47] and the Semi-Implicit Method for Pressure-Linked Equations (SIMPLE)^[48] or the SIMPLE-Consistent (SIMPLEC)^[49] algorithms, respectively, which can be selected.

The N -phase system of equations described in Section 2.2 are discretized using the FVM with support for unstructured meshes of general topology. Moreover, the code is equipped with dynamic load balancing (DLB) along with adaptive mesh refinement (AMR) techniques. Deploying this solution-adaptive approach allows to increase the mesh resolution dynamically where needed (at the interface) while keeping the computational load approximately balanced on parallel computations on distributed-memory computer architectures where domain decomposition is applied.

The system of equations described in Section 2.2 are applied to a series of validation cases in Section 4 to

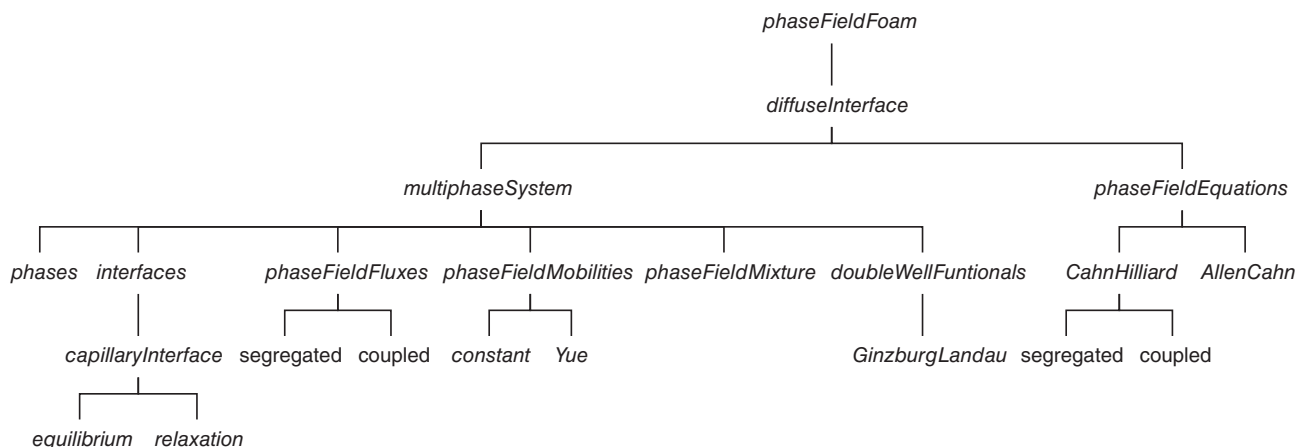


FIGURE 1 Structure of the *diffuseInterface* library

illustrate the capabilities of the software in the simulation of $N > 2$ immiscible phases. The discretization of the equations is performed using second order accurate schemes for both temporal and spatial terms. The advection terms (*divSchemes*), that is, the divergence terms for the scalar transport of the order parameters, are discretized using the high-resolution scheme *SuperBee*,^[50] while the convection term within the momentum equation is discretized using the second-order accurate *GammaV* scheme. The temporal discretization scheme (*ddtSchemes*) is set to a second-order accurate backward scheme. The gradient terms (*gradSchemes*) are discretized using the second order accurate *Gauss linear* scheme and the diffusion terms (*laplacianSchemes*) are discretized using the second order accurate *Gauss linear orthogonal* scheme.

4 | SIMULATION RESULTS

4.1 | Floating liquid lens

The floating liquid lens problem, which is considered a three-phase benchmark problem, is simulated here. This two-dimensional problem has been also studied in the works of Dong, Huang et al., and Yuan et al.^[21,22,26,27,51] In this problem, an initially circular liquid oil drop is floating on the air–water interface (see Figure 2) and will spread depending on the magnitude of the gravitational acceleration and interfacial tension coefficients. The simulation is performed until the oil drop reaches an equilibrium configuration. The final thickness of the drop will then be compared to an exact equilibrium solution given in the work of Huang et al.^[27] for the case when $|\mathbf{g}| = 0 \text{ m/s}^2$ and an asymptotic analysis provided by Langmuir and De Gennes et al.,^[52,53] viz.:

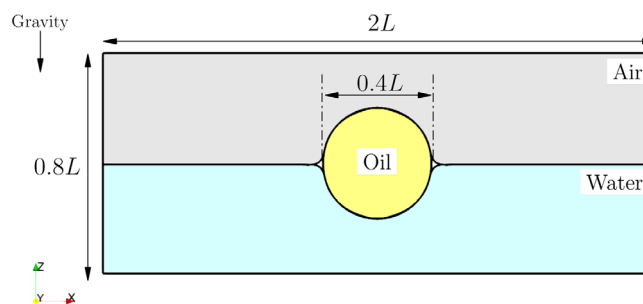


FIGURE 2 Schematic of the geometrical details of the floating liquid lens case

$$e_d = \sqrt{\frac{2(\sigma_{2,3} + \sigma_{1,2} - \sigma_{1,3})\rho_1}{\rho_2(\rho_2 - \rho_1)|\mathbf{g}|}}, \quad (13)$$

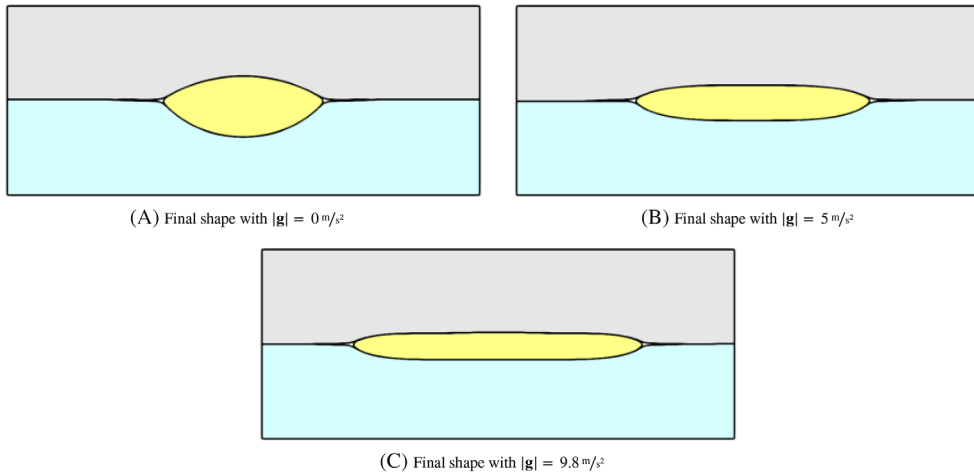
for all other values of the gravitational acceleration.

The transport properties of the fluids are shown in Table 1.

The computational domain is $[-L, L] \times [0, 0.8L]$ with the length scale $L = 0.04 \text{ m}$. The wall (no-slip) boundary condition is applied to the upper and lower boundaries, the *cyclic* (periodic) boundary condition is applied at the left and right boundaries, and the *empty* boundary condition is applied to the front and back boundaries, given that the computational domain is 2D.

The capillary width is $\varepsilon = 0.01L$ where the Cahn number is selected to be equal to 0.01 ($Cn = \frac{\varepsilon}{L}$). The planar computational domain is discretized by $[201 \times 81]$ cells, which results in approximately 16 interfacial cells ($N_c \approx 16$) at the interfaces. The mobility parameter is set to be $M = \chi \times \varepsilon^2$ with the constant $\chi = 0.1 \text{ m}^3 \text{ s/kg}$. An adaptive time stepping criteria is utilized where the time step is adjusted based on the maximum Courant number (Co_{\max}), which is limited to 0.2 with an initial time step

Property	Phase 1: Water	Phase 2: Oil	Phase 3: Air
Density (kg/m^3)	998.207	557	1.2041
Kinematic viscosity (m^2/s)	1.0038×10^{-6}	1.6424×10^{-4}	1.4782×10^{-5}
Interfacial tension coefficient (kg/s^2)	$\sigma_{1,2} = 0.04$	$\sigma_{1,3} = 0.0728$	$\sigma_{2,3} = 0.055$

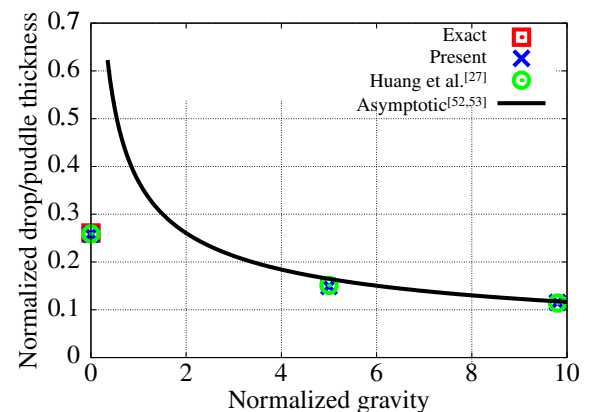
TABLE 1 Transport properties–floating liquid lens

FIGURE 3 Contours of order parameter–floating liquid lens

of $\Delta t = 10 \mu\text{s}$. The system is initialized with no initial velocity at $t = 0 \text{ s}$ and the simulations are performed until $t = 2 \text{ s}$ where an equilibrium state is reached.

Similar to the work of Huang et al.^[27] we have also considered three different magnitudes for the gravitational acceleration, which are (0, 5, 9.8) m/s^2 in the negative Z-direction.

Figure 3 depicts the final configuration of the three-phase system after reaching an equilibrium state corresponding to different magnitudes of the gravitational acceleration. The final shape of the air–oil–water system depends strongly on the interaction of the magnitude of the gravitational acceleration, pair-wise interfacial tension coefficient, and also the influence of fluid densities.^[22] As the value of the gravitational acceleration increases further, the final thickness of the drop at the centre point in the longitudinal direction reduces. In the event where the interfacial tension dominates, that is, $|\mathbf{g}| = 0 \text{ m/s}^2$, the oil drop resembles two circular ‘caps’ in the upper and lower regions, which is in agreement with the work of De Gennes et al.^[53] and in the event where the gravity dominates, the oil drop resembles a ‘puddle’.

Figure 4 shows the normalized drop/puddle thickness versus the normalized gravity. The drop/puddle thickness is normalized with respect to the length scale L and the gravity is normalized with respect to $|\mathbf{g}| = 1 \text{ m/s}^2$. The final maximum thickness is measured between the upper and lower interfaces of the equilibrium configuration in the vertical direction. It is observed in Figure 4 that our


FIGURE 4 Normalized thickness of the floating liquid lens versus normalized gravity

numerical results are in excellent quantitative agreement with the exact and asymptotic solutions.

4.2 | Rising bubble in two stratified layers

Here we consider the three-phase rising bubble in two stratified layers problem studied in the works of Boyer and Lapuerta, Boyer et al., and Fontes^[11,13,54] where a single air bubble of a specified volume rises initially in a heavy fluid and attempts to cross the interface between a heavy and a light fluid. Depending on the bubble volume,

it can either cross the fluid–fluid interface or remain captured at the interface. A criterion is proposed in the works of Greene et al.^[55,56] that predicts the state of the bubble at the interface depending on a critical volume, viz.

$$V^* = \left[\frac{2\pi \left(\frac{3}{4\pi}\right)^{\frac{1}{3}} \sigma_{1,2}}{|\mathbf{g}| (\rho_2 - \rho_3)} \right]^{\frac{3}{2}}. \quad (14)$$

For $V_{\text{bubble}} > V^*$ the air bubble will penetrate across the interface, while for $V_{\text{bubble}} < V^*$ it will be trapped at the interface. The criterion is based on ‘macroscopic balance between buoyancy and interfacial tension forces’^[13] and has been validated experimentally. It should be noted that the criterion only considers Archimede’s and interfacial tension forces and ignores hydrodynamic effects.^[11]

A schematic diagram illustrating the geometrical details of the rising bubble case setup is shown in Figure 5. The computational domain considered in this study is axisymmetric and has a dimension of $[0, D] \times [0, 10D]$, where D is the bubble initial diameter and the

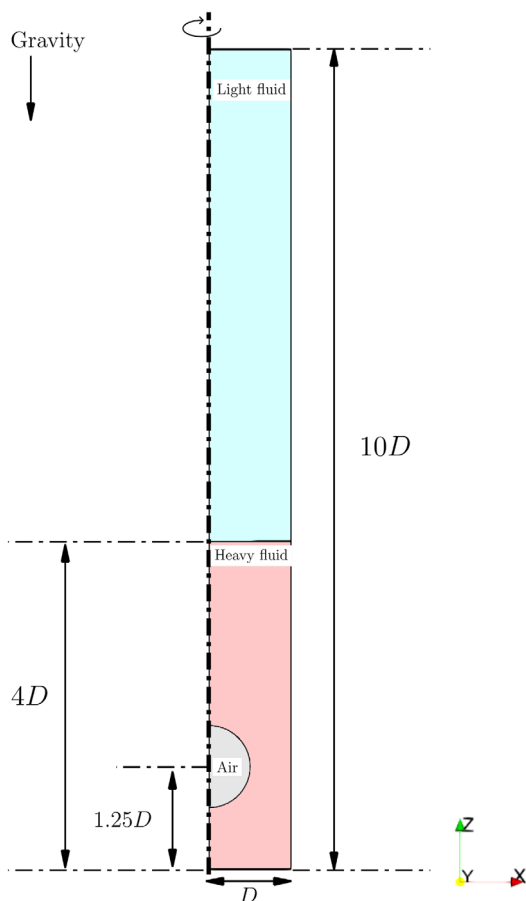


FIGURE 5 Schematic of the geometrical details of the rising bubbles case

gravity is applied in the negative Z -direction. The initial barycenter position of the air bubble is at $[0, 1.25D]$. The wall (no-slip) boundary condition is applied at the lower, upper, and the right boundaries, and the wedge boundary condition is applied at the left boundary.

The capillary width is $\varepsilon = 0.025D$ and the computational domain is discretized by $[80 \times 800]$ cells, resulting in $N_c \approx 8$ interfacial cells. The mobility parameter is set to be $M = \chi \times \varepsilon^2$ with the constant $\chi = 0.01 \text{ m} \cdot \text{s}/\text{kg}$. An adaptive time stepping criteria is utilized with the maximum Courant number $Co_{\text{max}} = 0.25$ and initial time step of $\Delta t = 0.001 \text{ s}$. The computational domain is initialized with zero initial velocity at $t = 0$.

The transport properties of the fluids are shown in Table 2.

Based on the transport properties of the fluids given in Table 2, Relation (14) gives the critical bubble radius $r^* \approx 2.7664 \text{ mm}$. In other words, an air bubble of radius $r_{\text{bubble}} > r^*$ can penetrate across the interface and an air bubble of radius $r_{\text{bubble}} < r^*$ remains trapped in the interface.

Based on the calculated r^* , we have performed numerical simulation for four different bubble radii, which are $r_{\text{bubble}} = 2.5, 3.0, 5.0, \text{ and } 7.0 \text{ mm}$. The numerical results are depicted in Figures 6–9, respectively. It should be pointed out that since the computational domain is axisymmetric, a rotational extrusion is performed for illustration of the bubble during the post-processing phase.

Both bubble penetration and entrapment are predicted successfully in our numerical simulations. It can be seen from Figure 6 that since $r_{\text{bubble}} < r^*$, the bubble is entrapped at the liquid–liquid interface. Figures 7–9 show bubble penetration through the liquid–liquid interface since $r_{\text{bubble}} > r^*$. It can also be seen that the penetrating bubble carries part of the heavy fluid into the light fluid domain in its wake (trailing edge), which is also seen in the works of Boyer and Lapuerta, Boyer et al., and Fontes^[11,13,54] and as the radius of the air bubble increases further, the length of the ‘heavy fluid tail’ becomes longer.

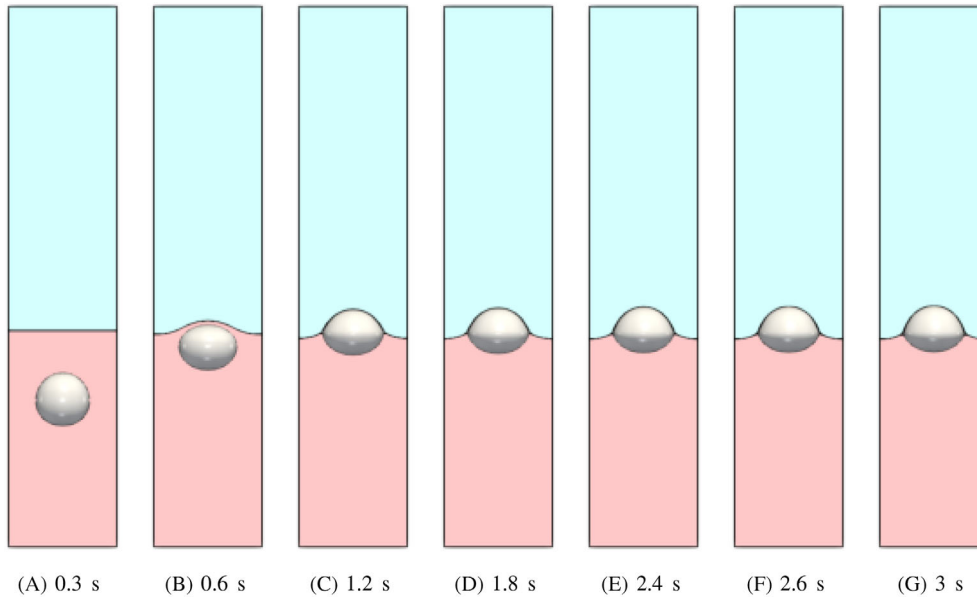
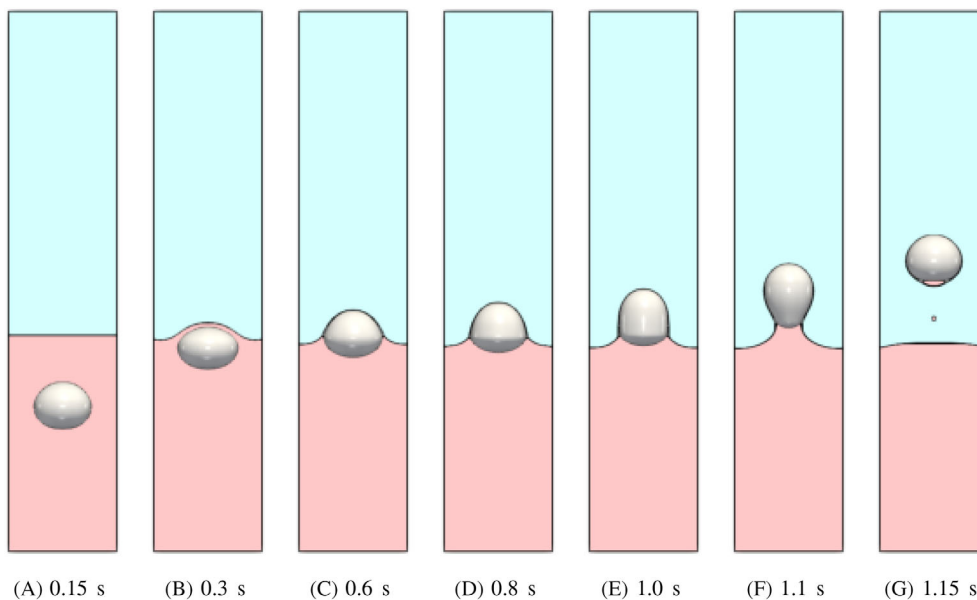
4.3 | A four phase problem

To illustrate the capabilities of the N -phase solver, the four phase fluid mixture problem proposed in the work of Dong^[22] has been simulated and the results are reported in this section. Here, the dynamics of four immiscible incompressible phases with transport properties as given in Table 3 is considered.

A schematic of the computational domain is illustrated in Figure 10. The computational domain is $[-L/2,$

Property	Phase 1: Heavy fluid	Phase 2: Light fluid	Phase 3: Air bubble
Density (kg/m^3)	1200	1000	1
Kinematic viscosity (m^2/s)	1.25×10^{-4}	1.0×10^{-4}	1.0×10^{-4}
Interfacial tension coefficient (kg/s^2)	$\sigma_{1,2} = 0.05$	$\sigma_{1,3} = 0.07$	$\sigma_{2,3} = 0.07$

TABLE 2 Transport properties—rising bubble in two stratified layers


 FIGURE 6 Contours of order parameter $\frac{\Gamma_{\text{bubble}}}{\Gamma^*} = 0.9037$

 FIGURE 7 Contours of order parameter $\frac{\Gamma_{\text{bubble}}}{\Gamma^*} = 1.0844$

$L/2] \times [0, 8 L/5]$ where the length scale $L = 0.02$ m and the gravity is applied in the negative Z -direction. The upper and lower boundaries are set to be *wall* (no-slip), the left and right boundaries are set to be *cyclic* (periodic), and the front and back boundaries are set to be *empty* since the case is 2D. The system is assumed to have zero initial velocity at $t = 0$ s.

The capillary width is $\varepsilon = 0.005 L$ and the planar computational domain is discretized by $[400 \times 640]$ cells, resulting in $N_c \approx 8$ interfacial cells. The mobility parameter is set to be $M = \chi \times \varepsilon^2$ with the constant $\chi = 0.001$ m · s/kg. We used an adaptive time stepping criteria where the time step is adjusted based on the maximum Courant number Co_{max} , which is limited to 0.2

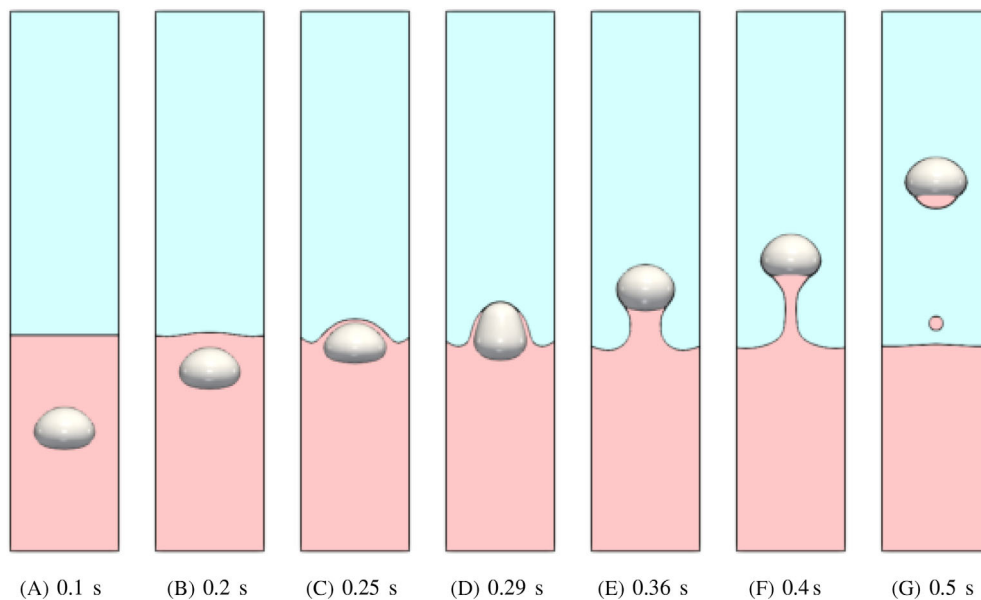
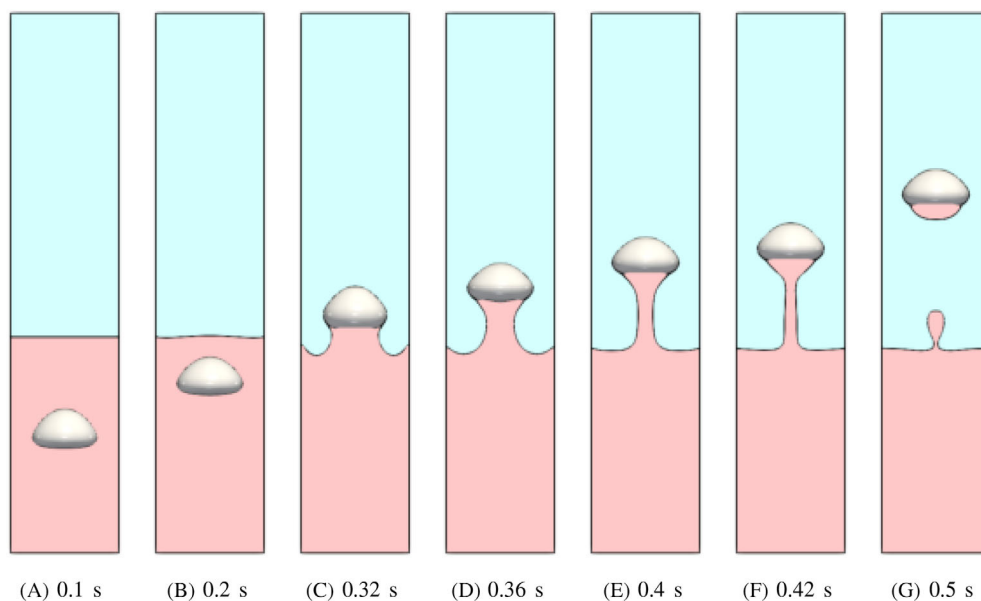
FIGURE 8 Contours of order parameter $\frac{\Gamma_{\text{bubble}}}{r} = 1.8074$

 FIGURE 9 Contours of order parameter $\frac{\Gamma_{\text{bubble}}}{r} = 2.5304$


TABLE 3 Transport properties—four phase mixture

Property	Phase 1: Air	Phase 2: Water	Phase 3: F1	Phase 4: F2
Density (kg/m ³)	1.2041	998.207	400	870
Kinematic viscosity (m ² /s)	1.4782×10^{-5}	1.0038×10^{-6}	5.0×10^{-5}	1.0517×10^{-4}
Interfacial tension coefficient (kg/s ²)	$\sigma_{1,2} = 0.0728$ $\sigma_{2,4} = 0.044$	$\sigma_{1,3} = 0.06$ $\sigma_{3,4} = 0.048$	$\sigma_{1,4} = 0.055$	$\sigma_{2,3} = 0.045$

with an initial time step of $\Delta t = 0.25 \mu\text{s}$. The system is initialized with no initial velocity at $t = 0$ s.

At $t = 0$ s, the upper half of the domain is filled with air, which contains the F2 drop, and the lower half of the domain is filled with water, which contains an air bubble and the F1 drop. When the system is released, the F2

drop free falls into the water through air and the air bubble and F1 drop move upward through the water.

Figure 11 depicts sequential time instances of the dynamics of the four phase mixture problem. In the upper half of the computational domain, gravity causes the F2 drop to descend rapidly through air, while

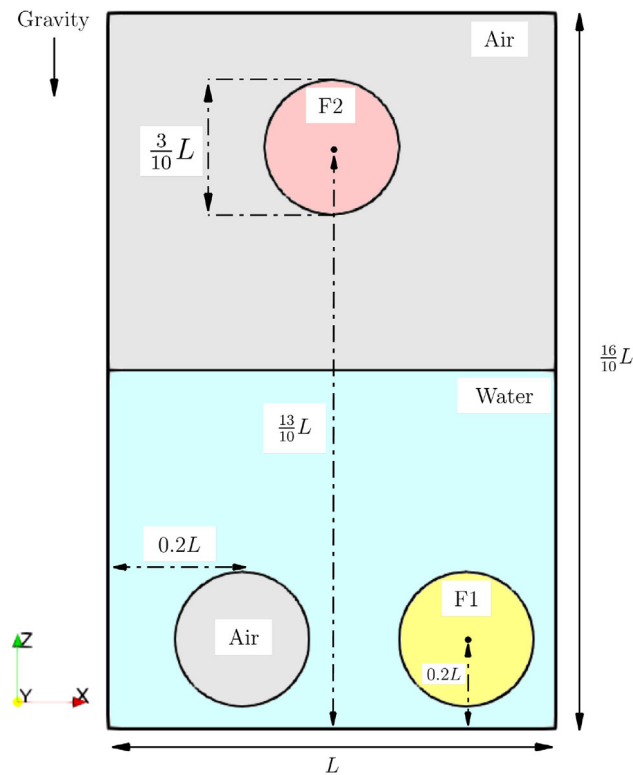


FIGURE 10 Schematic of the geometrical details of the four phase mixture case

maintaining its original circular shape, and impact the water surface. In the lower half of the computational domain, buoyancy causes the air bubble and the F1 drop to slowly ascend through water while deformation of the original circular shape of both phases is observed. At the moment of the impact of the F2 drop onto the water surface, an air pocket (trapped air) is formed beneath the F2 fluid. The air pocket remains trapped during the entire span of the simulation. The impact also generates outward-moving waves or ripples on the water surface. As a result of the small density contrast, fluid F2 remains floating but mostly submerged in water. The air bubble rises through water trying to join the air side of the computational domain. As the air bubble approaches the surface, it touches the F2 fluid, disconnects a portion of it from the water, escapes the water interface, and joins the air side of the domain. At the same time, the F1 fluid rises to the water surface and stays floating. By the end of the computation, the surface of the water is mainly covered by floating fluids of F1 and F2, which includes an air pocket. It is important to note that the characteristic features described in this section have been observed in the work of Dong.^[22] But a close inspection also reveals minor differences, such as the dynamics of the air bubble rupture at the free-surface at $t = 125$ ms (Figure 11E), which might be due to different numerical schemes used

and subtle differences in the underlying models related to reduction-consistency.

4.4 | Drop impact onto thin liquid film

The drop impact process of identical liquids is widely studied both experimentally^[43,57–71] and numerically.^[43,72–87] On the contrary, experiments conducted to describe the drop impact process onto thin liquid film of non-identical immiscible liquids are limited.^[88–92] By non-identical immiscible liquids, we explicitly mean that the film liquid is different from that of the drop and a homogeneous mixture is not formed when the liquids are mixed. The majority of the experimental studies focus on the impact morphology of miscible systems^[92–98] and typically the impact parameters are selected such that they lead to rim instabilities and, consequently, the generation of secondary droplets. To the best of our knowledge, even fewer numerical investigations of this complex process have been performed so far, such as the works of Yeganehdoust et al. and Wang et al.^[99,100] This can be due to complex impact dynamics of interfaces and the presence of triple-junction points.^[99,101] The work of Yeganehdoust et al.^[99] is concerned with a numerical study of the entrapped air layer when a water droplet of $D = 2$ mm impinges (Dupont Krytox103) film layer at three different Weber numbers and film thickness parameters. Wang et al.^[100] consider numerical computations of impact dynamics of a microsized water droplet falling onto an oil layer. Both studies utilize the VOF method for capturing the dynamics of interfaces.

The above discussion clearly shows the lack of numerical analysis covering drop impact process onto thin liquid films of immiscible liquids. Therefore, in this section we perform numerical computations of a silicone oil drop impacting onto a thin liquid film of water dyed with fuchsine (maroon coloured). Fuchsine does not bias the transport properties of water. The numerical results are compared to the in-house experimental results qualitatively. This study is a direct continuation of our previous work on drop-film interaction.^[43]

The experimental setup is shown in Figure 12. The setup consists of a drop generator system, an impact substrate wetted by a liquid film, as well as an optical system for recording the drop impact. The drop generated by the drop generator system is accelerated by gravity and impinges onto the liquid film. The substrate is a sapphire plate. A foil made of polyvinyl chloride with a recess of 50 mm in diameter and 0.6 mm in height is applied to the plate to contain the liquid film. The film thickness is precisely controlled by a confocal-chromatic film thickness sensor (Micro Epsilon confocalDT 2421 IFS 2405-1).

The optical system consists of a Photron SA-X2 chromatic high-speed camera and two high-performance LEDs (Constellation 120E). The LEDs in combination with a white screen in the background provide uniform

illumination. The drop impact is captured with a frame rate of 20 000 fps and a resolution of $16.5 \mu\text{m}$ per pixel. The surface tension between maroon coloured water and air $\sigma_{1,2} = 0.0728 \pm 0.003 \text{ kg/s}^2$ as well as the interfacial

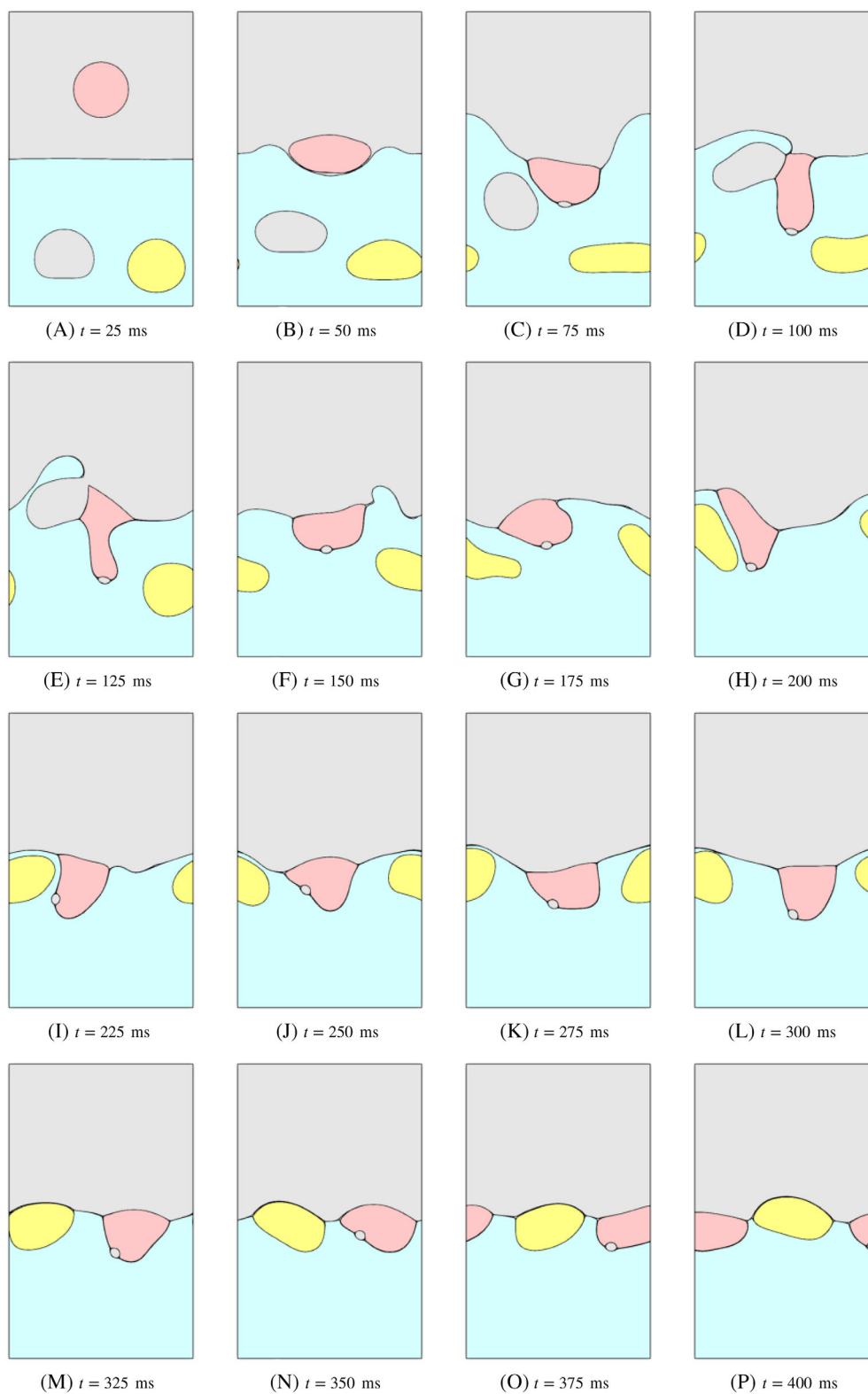


FIGURE 11 Contours of order parameter–four phase mixture problem

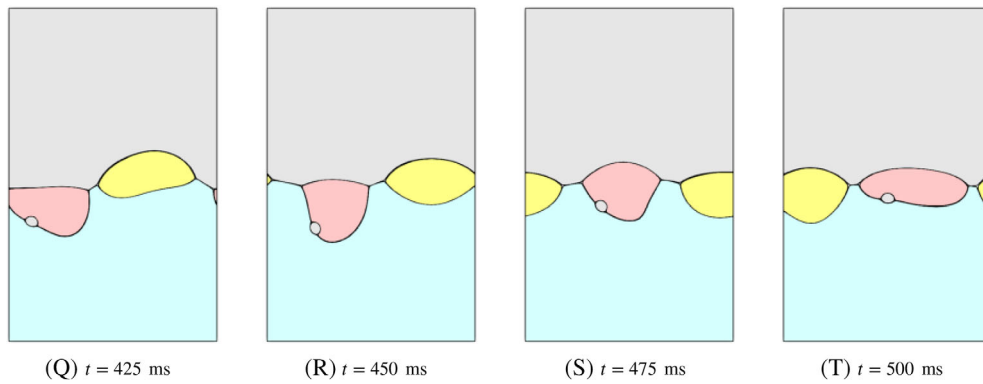


FIGURE 11 (Continued)

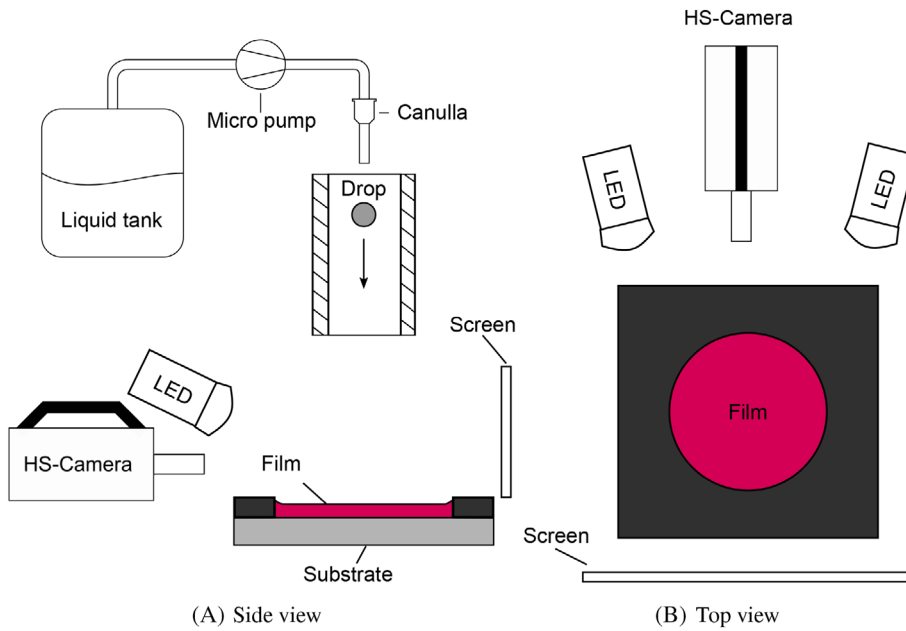


FIGURE 12 Schematic representation of the experimental setup in side and top view

Property	Phase 1: Air	Phase 2: Water	Phase 3: Silicone oil
Density (kg/m ³)	1.2041	998.207	930
Kinematic viscosity (m ² /s)	1.4782 × 10 ⁻⁵	1.0038 × 10 ⁻⁶	1.0 × 10 ⁻⁵
Interfacial tension coefficient (kg/s ²)	$\sigma_{1,2} = 0.0728$	$\sigma_{1,3} = 0.01829$	$\sigma_{2,3} = 0.027$

TABLE 4 Transport properties—drop impact onto thin liquid film

tension between maroon dyed water and silicone oil $\sigma_{2,3} = 0.027 \pm 0.003 \text{ kg/s}^2$ are measured with the DCAT 25 tensiometer from Dataphysics.

The transport properties of the liquids are shown in Table 4. In our study, the film height is $h = 0.5 \text{ mm}$ and the drop diameter is $D = 1.44 \text{ mm}$. This results in the film thickness parameter of $\delta = h/D = 0.35$ and the Ohnesorge number of $Oh = \mu_3/(\rho_3 D \sigma_{1,3})^{1/2} = 0.059$. The drop velocity is $U = 2 \text{ m/s}$ and, accordingly, the Weber number is $We = \rho_3 U^2 D / \sigma_{1,3} = 292.88$ and the Reynolds number is $Re = We^{0.5} / Oh = 288$.

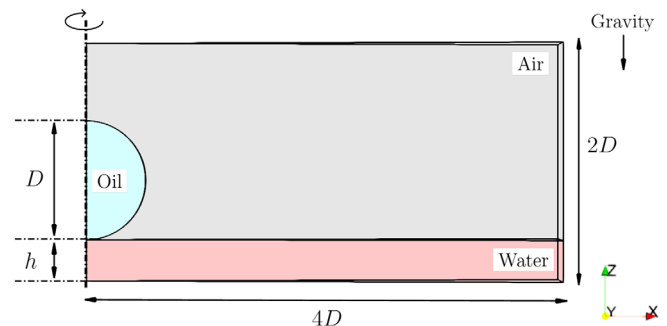


FIGURE 13 Schematic of the geometrical details of the drop impact case

The computational domain is depicted in Figure 13. The domain considered is axisymmetric with the dimensions of $[0, 4D] \times [0, 2D]$ where D is the drop diameter. The gravity

is applied in the negative Z-direction. The domain size is selected such that the effects of boundaries on the hydrodynamics of the process are excluded and all the topological

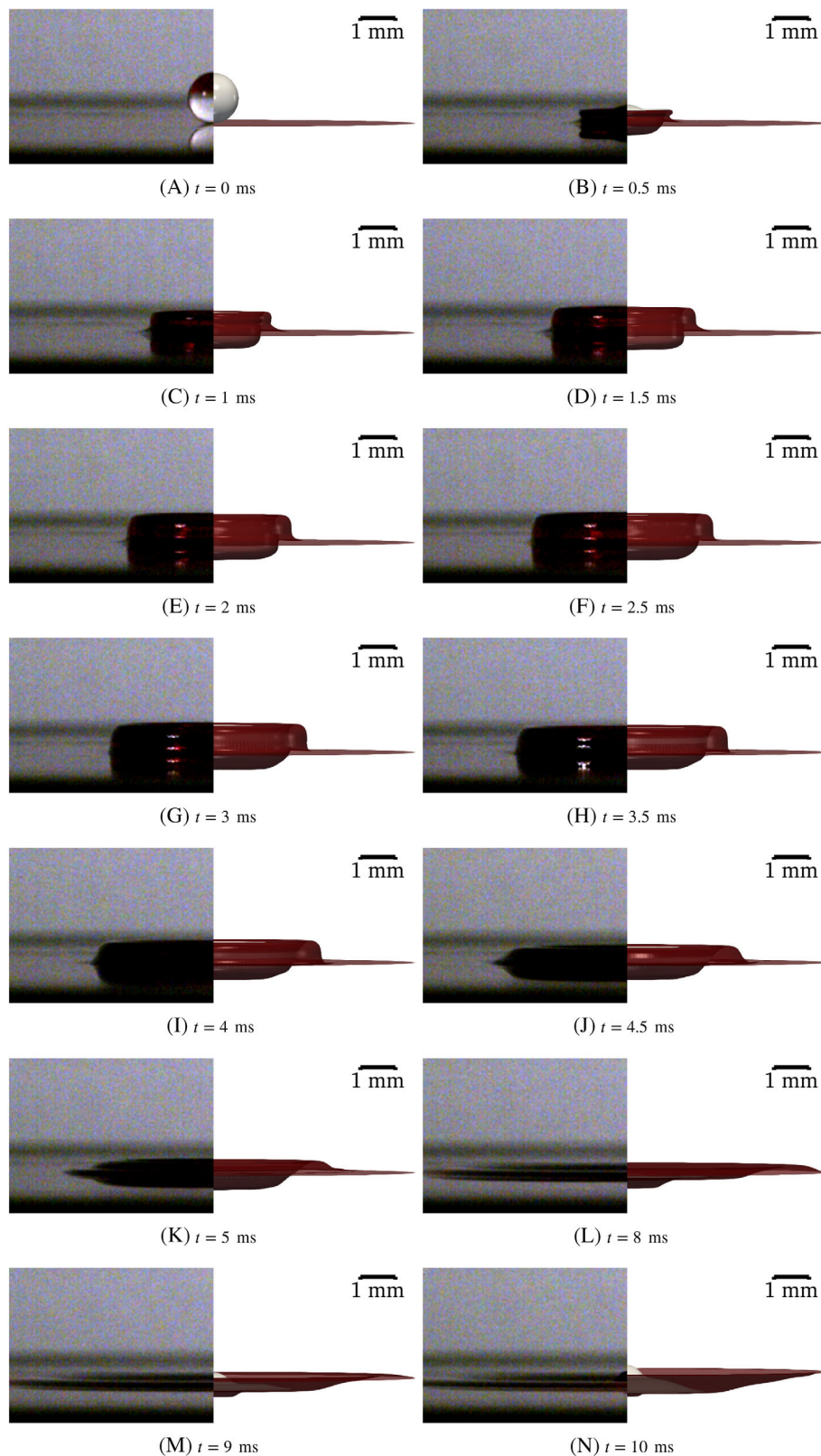


FIGURE 14 Recordings from the experiments (left) and simulation results (right)

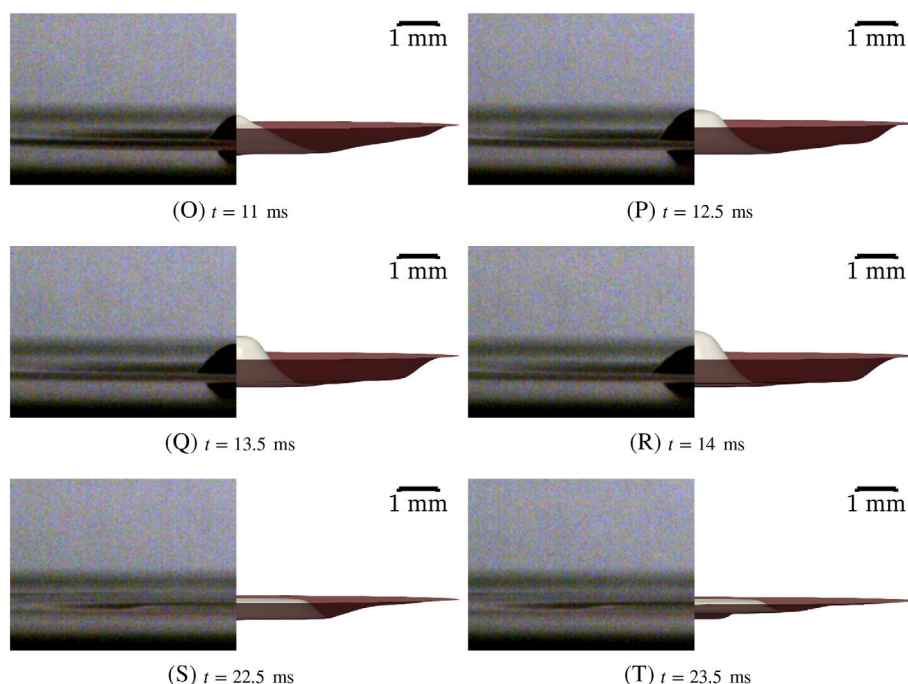


FIGURE 14 (Continued)

changes of the process are captured. The impacting drop is initialized very close to the liquid film. Justifications regarding the selected domain size and initial position of the impacting drop can be found in the work of Bagheri et al.^[43]

The capillary width is $\varepsilon = 0.01D$ and the mobility parameter is set to be $M = \chi \times \varepsilon^2$ with the constant $\chi = 0.001 \text{ m} \cdot \text{s}/\text{kg}$. The computational grid is generated with refinement regions that resolve the interfaces with approximately 16 interfacial cells during the entire time span of the simulation. This is vital in phase-field simulation of the drop impact onto thin liquid films since the interface profile affects calculation of the gradients of the order parameters and, thereupon, computation of the interfacial energies. The boundary conditions applied and the time stepping criteria employed are similar to those of our previous work.^[43]

Figure 14 depicts sequential time instances of the impact process where the experiment (left) is compared side by side to the simulation (right). Rotational extrusion is used for the post-processing of the numerical results and better visualization of the impact process. Moreover, the liquid film (water-fuchsine) is coloured maroon to represent the experiment realistically and to be distinguished from the grey impacting oil drop. We also reduced the opacity of the liquid film to 45% so that the topological changes that the oil drop undergoes can be visualized clearly in Figure 14.

The topological changes of the drop impact process for identical liquids include the coalescence of the

impacting drop and the liquid film in the early stages of the impact phenomenon. This is completely different for the case of non-identical liquids. Since the liquids are immiscible, the interfaces experience compression at the bottom half of the impacting drop and expansion at the upper half of the impacting drop. This clearly causes alteration of the initially specified capillary width ε and directly changes the interfacial energy associated with the interfaces. To address the accurate calculation of the interfacial mixing energy density parameter, we utilized our relaxation methodology developed in previous work^[43] to estimate an out-of-equilibrium mixing energy density parameter. Through numerical investigation, we found that the equilibrium formulation of $\lambda_{p,q}$ results in the incorrect prediction of the dynamics of the impact process.

As depicted in Figure 14, the crown rises as a result of a kinematic discontinuity caused by the jump in both the liquid film thickness and the local velocity field.^[102,103] The crown wall expansion is dominated by both the outer lamella sheet, which consists of water, and the inner lamella sheet, which consists of silicone oil. It can be seen from the simulation results that the crater widening is mainly due to the existence of the inner oil lamella sheet. The free rim, which restricts the crown wall expansion from above, consists of two layers of both liquids. In other words, there exist two free rims in this process. The crater descends as the interfacial tension forces become dominant compared to the inertial force. At the end of

the impact process a dome-like structure consisting of the impacting drop liquid is formed. This structure can change to a central (Worthington) jet at higher Weber numbers. The final configuration of this impact process is an oil disk floating on the water surface. It can be seen from Figure 14 that the entire process is captured very well by the numerical method described in this paper.

5 | SUMMARY AND OUTLOOK

In this contribution, we have performed exhaustive validation of our new phase-field solver for an arbitrary number ($N \geq 2$) of fluid phases against a broad bandwidth of different literature-known numerical tests and benchmarks for multiphase flows including a floating liquid lens and bubble rise in two stratified layers. The accuracy of the implemented diffuse-interface model has been shown for $N = 3$ phases against the aforementioned problems. The numerical method also showed a very good qualitative agreement against in-house experimental study of drop impact onto thin liquid film for non-identical immiscible liquids. We have demonstrated the potential of the method for simulation of $N = 4$ phases. The main objective has been to substantiate the physical fidelity of our new diffuse-interface model library and solver, demonstrating suitability for flows of multiple fluid phases, using the FVM with support for unstructured meshes of general topology in OpenFOAM (FOAM-extend 4.0/4.1).

In future work, we will build on this development aiming at simulations of multiphase flows in geometrically complex domains such as porous media or fibre mats. We will also extend our methodology to simulate miscible systems and enhance the computational efficiency by proper utilization of load-balanced AMR techniques.

AUTHOR CONTRIBUTIONS

Milad Bagheri: Conceptualization; data curation; formal analysis; investigation; methodology; software; validation; visualization; writing – original draft; writing – review and editing. **Bastian Stumpf:** Conceptualization; data curation; investigation; methodology; visualization; writing – review and editing. **Ilia V. Roisman:** Conceptualization; funding acquisition; methodology; project administration; resources; supervision. **Abdolrahman Dadvand:** Conceptualization; formal analysis; investigation; methodology; writing – review and editing. **Martin Wörner:** Conceptualization; formal analysis; funding acquisition; investigation; methodology; project administration; resources; supervision; writing – review and editing. **Holger Marschall:** Conceptualization; data

curation; formal analysis; funding acquisition; investigation; methodology; project administration; resources; software; supervision; validation; writing – review and editing.

ACKNOWLEDGEMENTS

This work was funded by the Deutsche Forschungsgemeinschaft (DFG, German Research Foundation) project number 237267381 SFB/Transregio 150 sub-projects A02 and B08. Part of the calculations for this research were conducted on the Lichtenberg High Performance Computer of the TU Darmstadt. Open Access funding enabled and organized by Projekt DEAL.







PEER REVIEW

The peer review history for this article is available at <https://publons.com/publon/10.1002/cjce.24510>.

DATA AVAILABILITY STATEMENT

Data available on request from the authors.

ORCID

Milad Bagheri  <https://orcid.org/0000-0003-4172-3187>
Bastian Stumpf  <https://orcid.org/0000-0002-6334-9766>
Ilia V. Roisman  <https://orcid.org/0000-0002-9878-3650>
Abdolrahman Dadvand  <https://orcid.org/0000-0002-6642-6122>
Martin Wörner  <https://orcid.org/0000-0003-4630-9292>
Holger Marschall  <https://orcid.org/0000-0001-8684-0681>

REFERENCES

- [1] J. W. Cahn, J. E. Hilliard, *J. Chem. Phys.* **1958**, 28, 258.
- [2] J. U. Brackbill, D. B. Kothe, C. Zemach, *J. Comput. Phys.* **1992**, 100, 335.
- [3] J. J. Feng, C. Liu, J. Shen, P. Yue, in *Modeling of Soft Matter* (Eds: M. C. T. Calderer, A. Seheel), Springer, New York **2005**, p. 1.
- [4] J. Lowengrub, L. Truskinovsky, *Proc. R. Soc. London, Ser. A* **1998**, 454, 2617.
- [5] D. Jacqmin, *J. Comput. Phys.* **1999**, 155, 96.
- [6] D. Jacqmin, *J. Fluid Mech.* **2000**, 402, 57.
- [7] C. Liu, J. Shen, *Phys. D* **2003**, 179, 211.
- [8] P. Yue, J. J. Feng, C. Liu, J. Shen, *J. Fluid Mech.* **2004**, 515, 293.
- [9] H. Ding, P. D. M. Spelt, C. Shu, *J. Comput. Phys.* **2007**, 226, 2078.
- [10] J. Kim, J. Lowengrub, *Interfaces and Free Boundaries* **2005**, 7, 435.
- [11] F. Boyer, C. Lapuerta, *ESAIM: Math. Modell. Numer. Anal.* **2006**, 40, 653.
- [12] J. Kim, *Computer Methods in Applied Mechanics and Engineering* **2007**, 196, 4779.
- [13] F. Boyer, C. Lapuerta, S. Minjeaud, B. Piar, M. Quintard, *Transp. Porous Media* **2010**, 82, 463.

- [14] Q. He, Y. Li, W. Huang, Y. Hu, D. Li, Y. Wang, *Computers & Mathematics with Applications* **2020**, *80*, 2830.
- [15] COMSOL, *Microfluidics Module User's Guide* (COMSOL 5.4), COSMOL Multiphysics, Stockholm, Sweden **2018**.
- [16] PELICANS, *Collaborative Development Environment* (Version 3.8.1), France **2021**, <https://gforge.irsn.fr/gf/project/pelicans/fr/> (accessed: June 15, 2022).
- [17] M. Řehoř, J. Blechta, O. Souček, *International Journal of Advances in Engineering Sciences and Applied Mathematics* **2017**, *9*, 30.
- [18] A. Logg, K. A. Mardal, G. Wells, *Automated Solution of Differential Equations by the Finite Element Method: The FEniCS Book*, Vol. 84, Springer Science & Business Media, Berlin and Heidelberg, Germany **2012**.
- [19] H. G. Lee, J. W. Choi, J. Kim, *Phys. A* **2012**, *391*, 1009.
- [20] F. Boyer, S. Minjeaud, *Math. Models Methods Appl. Sci.* **2014**, *24*, 2885.
- [21] S. Dong, *J. Comput. Phys.* **2014**, *276*, 691.
- [22] S. Dong, *J. Comput. Phys.* **2015**, *283*, 98.
- [23] H. G. Lee, J. Kim, *Phys. A* **2015**, *423*, 33.
- [24] S. Dong, *J. Comput. Phys.* **2018**, *361*, 1.
- [25] S. Wu, J. Xu, *J. Comput. Phys.* **2017**, *343*, 10.
- [26] S. Dong, *J. Comput. Phys.* **2017**, *338*, 21.
- [27] Z. Huang, G. Lin, A. M. Ardekani, ArXiv preprint **2020**, 2010.01099, <https://arxiv.org/abs/2010.01099> (accessed: April 5, 2021).
- [28] Z. Huang, G. Lin, A. M. Ardekani, ArXiv preprint **2020**, 2010.01738, <https://arxiv.org/abs/2010.01738> (accessed: September 4, 2021).
- [29] Y. Hu, D. Li, Q. He, *Int. J. Multiphase Flow* **2020**, *132*, 103432.
- [30] V. L. Ginzburg, L. D. Landau, *Zh. Eksp. Teor. Fiz.* **1950**, *20*, 1064.
- [31] A. Dadvand, M. Bagheri, N. Samkhaniani, H. Marschall, M. Wörner, *Phys. Fluids* **2021**, *33*, 053311.
- [32] D. J. Eyre, *MRS Online Proc. Libr.* **1998**, *529*, 39.
- [33] Z. Huang, G. Lin, A. M. Ardekani, *J. Comput. Phys.* **2021**, *434*, 110229.
- [34] C. Gugenberger, R. Spatschek, K. Kassner, *Phys. Rev. E* **2008**, *78*, 016703.
- [35] H. G. Weller, G. Tabor, H. Jasak, C. Fureby, *Comput. Phys.* **1998**, *12*, 620.
- [36] G. Chen, Q. Xiong, P. J. Morris, E. G. Paterson, A. Sergeev, Y. C. Wang, *Notices of the American Mathematical Society* **2014**, *61*, 354.
- [37] F. Moukalled, L. Mangani, M. Darwish, *Computational Fluid Dynamics: An Advanced Introduction with OpenFOAM® and Matlab*. The Finite Volume Method, Vol. 113, Springer International Publishing, Cham, Switzerland **2016**, p. 103.
- [38] X. Cai, H. Marschall, M. Wörner, O. Deutschmann, *Chem. Eng. Technol.* **2015**, *38*, 1985.
- [39] X. Cai, M. Wörner, H. Marschall, O. Deutschmann, *Catal. Today* **2016**, *273*, 151.
- [40] V. Fink, X. Cai, A. Stroh, R. Bernard, J. Kriegseis, B. Frohnapfel, H. Marschall, M. Wörner, *Int. J. Heat Fluid Flow* **2018**, *70*, 271.
- [41] M. Wörner, N. Samkhaniani, X. Cai, Y. Wu, A. Majumdar, H. Marschall, B. Frohnapfel, O. Deutschmann, *Applied Mathematical Modelling* **2021**, *95*, 53.
- [42] N. Samkhaniani, A. Stroh, M. Holzinger, H. Marschall, B. Frohnapfel, M. Wörner, *Int. J. Heat Mass Transfer* **2021**, *180*, 121777.
- [43] M. Bagheri, B. Stumpf, I. V. Roisman, C. Tropea, J. Hussong, M. Wörner, H. Marschall, *Int. J. Heat Fluid Flow* **2022**, *94*, 108943.
- [44] F. Jamshidi, H. Heibel, M. Hasert, X. Cai, O. Deutschmann, H. Marschall, M. Wörner, *Comput. Phys. Commun.* **2019**, *236*, 72.
- [45] S. S. Deshpande, L. Anumolu, M. F. Trujillo, *Comput. Sci. Discovery* **2012**, *5*, 014016.
- [46] D. Jamet, D. Torres, J. U. Brackbill, *J. Comput. Phys.* **2002**, *182*, 262.
- [47] R. I. Issa, *J. Comput. Phys.* **1986**, *62*, 40.
- [48] S. V. Patankar, D. B. Spalding, *Int. J. Heat Mass Transfer* **1972**, *15*, 1787.
- [49] J. P. Van Doormaal, G. D. Raithby, *Numerical Heat Transfer* **1984**, *7*, 147.
- [50] P. L. Roe, *Large-Scale Computations in Fluid Mechanics*. Lectures in Applied Mathematics, Vol. 22, American Mathematical Society, Providence, RI **1985**, p. 163.
- [51] X. Yuan, H. Liang, Z. Chai, B. Shi, *Phys. Rev. E* **2020**, *101*, 063310.
- [52] I. Langmuir, *J. Chem. Phys.* **1933**, *1*, 756.
- [53] P. G. De Gennes, F. Brochard-Wyart, D. Quéré, *Capillarity and Wetting Phenomena: Drops, Bubbles, Pearls, Waves*, Vol. 315, Springer, New York **2004**.
- [54] Simulate three-phase flow with a new phase field interface, COMSOL Blog, <https://www.comsol.com/blogs/simulate-three-phase-flow-with-a-new-phase-field-interface/> (accessed: June 2022).
- [55] G. A. Greene, J. C. Chen, M. T. Conlin, *Int. J. Heat Mass Transfer* **1988**, *31*, 1309.
- [56] G. A. Greene, J. C. Chen, M. T. Conlin, *Int. J. Heat Mass Transfer* **1991**, *34*, 149.
- [57] M. Rein, *Fluid Dynamics Research* **1993**, *12*, 61.
- [58] G. E. Cossali, A. Coghe, M. Marengo, *Exp. Fluids* **1997**, *22*, 463.
- [59] A. Coghe, G. Brunello, G. E. Cossali, M. Marengo, in *ILASS Europe 99*, Vol. 99, ILASS – Europe, Toulouse, France **1999**.
- [60] G. E. Cossali, G. Brunello, A. Coghe, M. Marengo, in *Italian Congress of Thermo-fluid Dynamics UIT, Ferrara*, Vol. 30, Università degli studi, Ferrara, Italy **1999**, pp. 1–12.
- [61] A. B. Wang, C. C. Chen, *Phys. Fluids* **2000**, *12*, 2155.
- [62] I. V. Roisman, C. Tropea, *J. Fluid Mech.* **2002**, *472*, 373.
- [63] S. T. Thoroddsen, T. G. Etoh, K. Takehara, *J. Fluid Mech.* **2003**, *478*, 125.
- [64] R. Rioboo, C. Bauthier, J. Conti, M. Voue, J. De Coninck, *Exp. Fluids* **2003**, *35*, 648.
- [65] A. L. Yarin, *Annu. Rev. Fluid Mech.* **2006**, *38*, 159.
- [66] C. Motzkus, F. Gensdarmes, E. Géhin, *J. Aerosol Sci.* **2009**, *40*, 680.
- [67] G. Coppola, G. Rocco, L. d. Luca, *Phys. Fluids* **2011**, *23*, 022105.
- [68] N. L. Hillen, J. S. Taylor, C. Menchini, G. Morris, M. Dinc, D. D. Gray, J. Kuhlman, in *43rd AIAA Fluid Dynamics Conf.*, The American Institute of Aeronautics and Astronautics (AIAA), San Diego, CA **2013**. <https://doi.org/10.2514/6.2013-2976>

- [69] G. Liang, I. Mudawar, *Int. J. Heat Mass Transfer* **2016**, 101, 577.
- [70] S. Kitabayashi, K. Enoki, T. Okawa, in *Int. Conf. Nuclear Engineering*, Vol. 57878, American Society of Mechanical Engineers, Shanghai, China **2017**.
- [71] B. Chen, R. Tian, F. Mao, *Ann. Nucl. Energy* **2020**, 136, 107038.
- [72] C. Josserand, S. Zaleski, *Phys. Fluids* **2003**, 15, 1650.
- [73] H. Xie, S. Koshizuka, Y. Oka, *Int. J. Numer. Methods Fluids* **2004**, 45, 1009.
- [74] N. Nikolopoulos, A. Theodorakakos, G. Bergeles, *J. Comput. Phys.* **2007**, 225, 322.
- [75] S. Zy, Y. Yan, Y. Fan, Y. Qian, G. Hu, *Journal of Hydrodynamics, Series B* **2008**, 20, 267.
- [76] S. H. Lee, N. Hur, S. Kang, *J. Mech. Sci. Technol.* **2011**, 25, 2567.
- [77] T. Jiang, J. Ouyang, X. Li, J. Ren, X. Wang, *J. Appl. Mech. Tech. Phys.* **2013**, 54, 720.
- [78] Y. Guo, L. Wei, G. Liang, S. Shen, *Int. Commun. Heat Mass Transfer* **2014**, 53, 26.
- [79] G. Liang, Y. Guo, S. Shen, Y. Yang, *Theor. Comput. Fluid Dyn.* **2014**, 28, 159.
- [80] H. Shetabivash, F. Ommi, G. Heidarinejad, *Phys. Fluids* **2014**, 26, 012102.
- [81] G. Yali, W. Lan, S. Shengqiang, C. Guiying, *Int. J. Low-Carbon Technol.* **2014**, 9, 150.
- [82] C. Josserand, P. Ray, S. Zaleski, *J. Fluid Mech.* **2016**, 802, 775.
- [83] S. F. Kharmani, M. Passandideh-Fard, H. Niazmand, *J. Mol. Liq.* **2016**, 222, 1172.
- [84] C. Liu, M. Shen, J. Wu, *J. Mec. Theor. Appl.* **2018**, 67, 269.
- [85] T. Kondo, K. Ando, *Phys. Fluids* **2019**, 31, 013303.
- [86] T. Xavier, D. Zuzio, M. Averseng, J. L. Estivalezes, *Meccanica* **2020**, 55, 387.
- [87] M. R. Rezaie, M. Norouzi, M. H. Kayhani, S. M. Taghavi, *Meccanica* **2021**, 56, 2021.
- [88] N. Chen, H. Chen, A. Amirfazli, *Phys. Fluids* **2017**, 29, 092106.
- [89] Z. Che, O. K. Matar, *Soft Matter* **2018**, 14, 1540.
- [90] H. M. Kittel, I. V. Roisman, C. Tropea, in *Selected Papers from the 31st Int. Congress High-Speed Imaging Photonics* (Eds: T. Goji Etoh, H. Shiraga), Vol. 10328, SPIE (Society of Photo-Optical Instrumentation Engineers), Bellingham, WA **2017**.
- [91] D. F. S. Ribeiro, A. R. R. Silva, M. R. O. Panão, *Appl. Sci.* **2020**, 10, 6698.
- [92] Y. Wu, Q. Wang, C. Y. Zhao, *Exp. Fluids* **2021**, 62, 1.
- [93] S. T. Thoroddsen, T. G. Etoh, K. Takehara, *J. Fluid Mech.* **2006**, 557, 63.
- [94] A. Geppert, A. Štrbac, M. Marengo, G. Lamanna, B. Weigand, Proc. Int. Conf. Liquid Atomization and Spray Systems, 13th ICLASS, Tainan, Taiwan, August **2015**.
- [95] A. Geppert, A. Terzis, G. Lamanna, M. Marengo, B. Weigand, presented at 27th Annual Conf. Liquid Atomization Spray Systems, Brighton, UK, September **2016**.
- [96] H. Kittel, I. Roisman, C. Tropea, *ILASS 2017, 28th European Conf. Liquid Atomization Spray Systems*, Editorial Universitat Politècnica de València, Valencia, Spain **2017**, p. 716.
- [97] N. E. Ersoy, M. Eslamian, *Phys. Fluids* **2019**, 31, 012107.
- [98] N. E. Ersoy, M. Eslamian, *Exp. Therm. Fluid Sci.* **2020**, 112, 109977.
- [99] F. Yeganehdoust, R. Attarzadeh, I. Karimfazli, A. Dolatabadi, *Int. J. Multiphase Flow* **2020**, 124, 103175.
- [100] B. Wang, C. Wang, Y. Yu, X. Chen, *Phys. Fluids* **2020**, 32, 012003.
- [101] N. Tofighi, M. Yildiz, *Computers & Mathematics with Applications* **2013**, 66, 525.
- [102] A. L. Yarin, D. A. Weiss, *J. Fluid Mech.* **1995**, 283, 141.
- [103] A. L. Yarin, I. V. Roisman, C. Tropea, *Collision Phenomena in Liquids and Solids*, Cambridge University Press, Cambridge, UK **2017**.

AUTHOR BIOGRAPHIES



Milad Bagheri received his MSc degree in Computational Science and Engineering from the University of Rostock, Germany, in October 2019. He is currently a research associate and doctoral student in the Computational Multiphase Flow group in the

Mathematical Modeling and Analysis (MMA) institute at the Technical University of Darmstadt. His research belongs to subproject B08 in the transregional Collaborative Research Centre 150, funded by the German Research Foundation (DFG). The objective of his research is to develop a predictive diffuse-interface approach for multi-phase flows of miscible and immiscible multi-component fluids.



Bastian Stumpf is a research associate and doctoral student at the Institute for Fluid Mechanics and Aerodynamics at the Technical University of Darmstadt. Here, he is working on the Project ‘A02 – Drop/spray impact onto wall films of different liquids’, which is embedded in the Collaborative

Research Center 150 ‘Turbulent, chemically reactive, multiphase flows near walls’. The focus of his research has been the drop impact onto thin liquid films with one or more components since July 2019. In June 2019, he successfully completed his master’s degree in Mechanical and Process Engineering at the Technical University of Darmstadt.



Professor Ilia V. Roisman is based at the Institute of Fluid Mechanics and Aerodynamics at Technische Universität Darmstadt, where he heads the research group Dynamics of Drops and Sprays. He defended his DSc title in 1998 at the Technion–Israeli Institute of Technology. He was the

recipient of the STAB Prize for Fluid Mechanics in 2010. Ilia Roisman is the author of more than 120 journal publications, h-index 42. His research interests include problems of the physics of icing, spray cooling, drop impact, wetting of complex substrates, interfacial flows, atomization, etc.



Dr. Abdolrahman Dadvand was introduced to the field of Mechanical Engineering (Thermo-Fluids) in 1998, when he enrolled at Urmia University in Iran. After completing his BSc in Mechanical Engineering (Energy Conversion) in 2001, he advanced his training and education at the University of Tabriz, Iran, which culminated in the conferral of his MSc in 2004. Dr. Dadvand completed his advanced academic training at the University of Tabriz, where he earned a PhD in Mechanical Engineering (Energy Conversion) in 2009. During his PhD, Dr. Dadvand has also spent a period of 7 months at the National University of Singapore (NUS) doing experiments on the collapsing bubble-induced droplet generation. Since he finished his PhD, Dr. Dadvand has been employed as a full-time tenure track Assistant Professor at the Department of Mechanical Engineering, Urmia University of Technology (UUT), Iran, where he teaches courses in Fluid Mechanics, Computational Fluid Dynamics (CFD), Advanced Engineering Mathematics, Computer Programming, Multiphase Flows, etc. Dr. Dadvand is currently an associate professor at UUT. He was also a visiting professor at Karlsruhe Institute of Technology (KIT), Germany (2019–2021) working on Phase Field modelling of multiphase flows. Dr. Dadvand has published two book chapters, more than 60 papers in peer-reviewed journals, and more than 40 papers in national and international conferences.



Martin Wörner studied mechanical engineering at the University of Karlsruhe (TH), Germany. After graduating as an engineer (Dipl.-Ing.) in 1989, he received his doctoral degree (Dr.-Ing.) in 1994 at the same faculty. Throughout his professional career, he has worked at various institutes of today's Karlsruhe Institute of Technology (KIT) and its predecessor institutions, the Nuclear Research Center Karlsruhe and the Research Center Karlsruhe. His

current position is head of the Multiphase Flow Group at the Institute of Catalysis Research and Technology (IKFT) at KIT. His scientific interests are in the development of methods and computer codes for the numerical simulation of multi-phase flows and their utilization to study fundamental and technical aspects of two-phase flows in mechanical engineering and process engineering. Since 2003, Dr. Wörner has been lecturing on Numerical Modelling of Multiphase Flows at KIT.



Dr.-Ing. Holger Marschall studied chemical engineering at the Technical University of Munich (TUM), Germany. He graduated as engineer (Dipl.-Ing.) in 2006 and received his PhD in 2011 at the same university.

He is currently head of the research group Computational Multiphase Flow at Technical University of Darmstadt, Germany. Dr. Marschall is seeking to understand fundamental properties of multiphase systems. With his work, he aims to benefit chemical and biological processes, biomedical devices, and energy applications. For this, he develops high-fidelity simulation methods for the computer-aided prediction of the involved transport processes. His scientific focus is on the open-source C++ library OpenFOAM for computational continuum physics and multiphysics, where he is concerned with methods particularly suited for scale-bridging and/or coupled processes at interfaces. Dr. Marschall is active in organizing the International Conference on Numerical Methods in Multiphase Flows (ICNMMF) as well as the International OpenFOAM Workshop. He is an associate editor of *The Canadian Journal of Chemical Engineering* and editor of the *OpenFOAM Journal*. Dr. Marschall is assigned member of the DECHEMA ProcessNet Committee Computational Fluid Dynamics and he serves as the chair of the Technical Committee on Multiphase Flows within the official OpenFOAM governance structure.

How to cite this article: M. Bagheri, B. Stumpf, I. V. Roisman, A. Dadvand, M. Wörner, H. Marschall, *Can. J. Chem. Eng.* **2022**, 1. <https://doi.org/10.1002/cjce.24510>